Published in *Science* Vol. 291, no. 5501 (January 5, 2001), pp. 97–100; doi 10.1126/science.291.5501.97  http://www.sciencemag.org/cgi/content/full/291/5501/97

Submitted September 11, 2000; accepted 21 November 21, 2000.

# Atomically Resolved Single-Walled Carbon Nanotube Intramolecular Junctions

Min Ouyang,[1] Jin-Lin Huang,[1] Chin Li Cheung,[1] and Charles M. Lieber[1, 2,*]

[1] Department of Chemistry and Chemical Biology, Harvard University, Cambridge, MA 02138, USA.
[2] Division of Engineering and Applied Sciences, Harvard University, Cambridge, MA 02138, USA.
* Corresponding author; email: cml@cmliris.harvard.edu

Intramolecular junctions in single-walled carbon nanotubes are potentially ideal structures for building robust, molecular-scale electronics but have only been studied theoretically at the atomic level. Scanning tunneling microscopy was used to determine the atomic structure and electronic properties of such junctions in single-walled nanotube samples. Metal-semiconductor junctions are found to exhibit an electronically sharp interface without localized junction states, whereas a more diffuse interface and low-energy states are found in metal-metal junctions. Tight-binding calculations for models based on observed atomic structures show good agreement with spectroscopy and provide insight into the topological defects forming intramolecular junctions. These studies have important implications for applications of present materials and provide a means for assessing efforts designed to tailor intramolecular junctions for nanoelectronics.

Single-walled carbon nanotubes (SWNTs) intramolecular junctions (IMJs) formed by interposing one or multiple topologic pentagon-heptagon (5–7) defects (in the normal hexagonal structure) between two nanotube segments of different helicity have aroused substantial interest due to their potential for creating nanoelectronic devices (1–3). Theoretical studies of the electronic properties of model SWNT IMJs (4–9) suggest that these structures could function as molecular-size metal-semiconductor (M-S), metal-metal (M-M), or semiconductor-semiconductor building blocks with robust solid-state behavior. To date, experimental observations of bent SWNTs (10, 11) and transport through nanotube structures (11, 12) have provided only indirect evidence for the existence of IMJs. Atomically resolved scanning tunneling microscopy (STM), which has previously shown that SWNTs can exhibit a wide range of atomic structures (13–15), represents a potentially ideal technique for illuminating the properties of IMJs. The wide range of SWNT structures observed (15) underscores the importance in elucidating the atomic-level structure of suspected IMJs to define their existence (16) and to understand their electronic properties.

We report STM studies of SWNTs that resolve the atomic structures and electronic properties of M-S and M-M IMJs. The observed atomic structures of the SWNTs forming IMJs were used to construct atomic models of the junctions. Comparisons between tight-binding calculations and spatially resolved tunneling spectroscopy data were used to determine the most likely configurations of topological defects for IMJs and reveal characteristic features of the M-S and M-M IMJs. The ability to characterize IMJs at the atomic level will aid in further developing our understanding of these molecular-scale structures and will be critical to synthetic efforts aimed at "engineering" junctions.

A homemade ultrahigh vacuum STM operating at 5 K was used to characterize the structure and electronic properties of SWNTs. Sample preparation and image analysis were similar to previous studies (14, 17). Atomically resolved images of a large number (about 100) of individual SWNTs and SWNT bundles were recorded, and about 10% of these were found to exhibit stable defect features under extended scanning. Features that change with scanning are also observed and can be attributed to adsorbates (18).

A typical example of a SWNT IMJ (Figure 1A), which is located at the center of the image, is visible at different bias voltages as a clear perturbation in the regular atomic-scale structure of the upper and lower portions of the SWNT. The fact that a 5–7 defect is not clearly visible in this region is not surprising because (i) the defect may not be located directly at the upper surface of the SWNT circumference and (ii) the local density of states, which are measured in the STM experiment, do not necessarily reflect the atom positions. This latter point has been addressed specifically in recent theoretical calculations of expected STM images for different 5–7 defect configurations (19–23). The presence of the IMJ is, however, demonstrated clearly by determining the SWNT structural indices, which are defined by the diameter and helicity, and the electronic properties (Figure 1B) for the upper and lower portions of the nanotube.

Analysis of Figure 1A shows that the upper and lower portions of the nanotube have similar diameters, $1.57 \pm 0.07$ nm, but significantly different in its chiral angles ($\theta$), where the angle is defined relative to the zigzag direction, for the upper and lower portions, $\theta = -3.9° \pm 0.8°$ and $-10.5° \pm 0.8°$, respectively. The very significant change in chiral angle that occurs across the local defect is strong evidence that this feature is an IMJ. Further support for this conclusion was obtained from tunneling spectroscopy data (Figure 1B), which show clear peaks corresponding to the van Hove singularities (VHS) characteristic of the one-dimensional SWNT (13–15). The difference between the first VHS in the upper segment, 0.45 eV, is about three times smaller than the difference for the lower segment, 1.29 eV, and is thus consistent with the upper and lower portions being semiconducting and metallic, respectively (15). That is, the gap, $E_g$, between first VHS depends only on diameter ($d$) and not the helicity: $E_g = G\gamma_0 a_{cc}/d$, where $\gamma_0$ is transfer matrix element, $a_{cc}$ is the carbon-carbon bond distance, and $G$ is 2 for semiconducting and 6 for metallic SWNTs (24). The gaps calculated using the measured diameter and our experimentally determined value of $\gamma_0 = 2.5$ eV (14, 24), 0.45 and 1.35 eV, are consistent with those measured (Figure 1B).

We also characterized in greater detail the electronic properties of the IMJ using spatially resolved spectroscopy measurements (Figure 1C). Examination shows that the gap defined by VHS in the semiconducting tube segment (small arrows) decays across the IMJ into the metallic segment within <1 nm, whereas the distinct spectroscopic features of the metallic tube (large arrows) appear to decay more quickly across the junction interface. The relatively sharp interface is consistent with theoretical calculations on model structures (5–8) and supports the idea that molecular-scale devices could be developed from SWNT IMJs. In addition, no localized states are detected in the interface region, suggesting that the M-S junction may behave as an ideal Schottky diode. These atomic-level observations lend support to recent experiments (11, 12) that have attributed IMJs to rectifying transport data.

In comparison to previous work (10–12), our atomically resolved images enable atomic models of the junction to be constructed, analyzed theoretically, and compared with the experimental spectroscopy data. To build models of the IMJ, the SWNT (n,m) indices that correspond to a specific combination of $d$ and $\theta$ (24) were determined by using an iterative projection matching method (17). The

(n,m) indices define the nanotube structure through the vector $\mathbf{C_h} = n\mathbf{a_1} + m\mathbf{a_2}$, where $\mathbf{a_1}$ and $\mathbf{a_2}$ are the unit vectors of the graphene hexagonal lattice. For the semiconducting and metallic portions, these indices are (21,–2) and (22,–5), respectively. SWNT segments with these indices can be joined seamlessly along a common axis using different configurations of 5–7 defects. Two low-energy structural models are shown (Figure 2A), which have been optimized using molecular mechanics energy minimization. Model I consists of three separated 5–7 pairs and Model II has two isolated 5–7 pairs and one 5–7/7–5 pair. It is possible to evaluate the viability of these atomic models by calculating the local electronic density of states (LDOS) and comparing these with experiment. The results from our tight-binding calculations (15, 25) (Figure 2B) show that LDOS for Model I matches the experimental data well. Specifically, the first VHS of the semiconducting segment decays across the IMJ into the metallic segment with a decay constant similar to that in the experiment. In contrast, the LDOS calculated for Model II exhibits low-energy states around –0.10 eV, which are not observed in our experimental data. Hence, we believe that Model I can be reasonably assigned to the structure for the observed IMJ. Our new results and previous calculations (5–8) show that the absence or presence of localized states at the M-S junction reflect the specific configuration of 5–7 defects. Because this could be used to vary device properties, it will be interesting to see whether these configurations can be controlled in the future.

We also characterized a M-M IMJ junction using similar methods (Figure 3). The atomically resolved image (Figure 3A) suggests a large difference in diameters but similar chiral angles for the upper and lower segments of IMJ structure, $d = 1.23 \pm 0.05$ nm and $\theta = 24.3° \pm 0.6°$, and $d = 1.06 \pm 0.05$ nm and $\theta = 23.8° \pm 0.6°$, respectively. The local spectroscopy data recorded away from the IMJ region (Figure 3B) demonstrates that the magnitude of the first VHS gap for the lower segment is larger than that recorded on the upper segment. Thus, these gaps are consistent with the diameters determined from the images. Moreover, they show that both segments are metallic SWNTs. In addition, spatially resolved spectroscopy data recorded

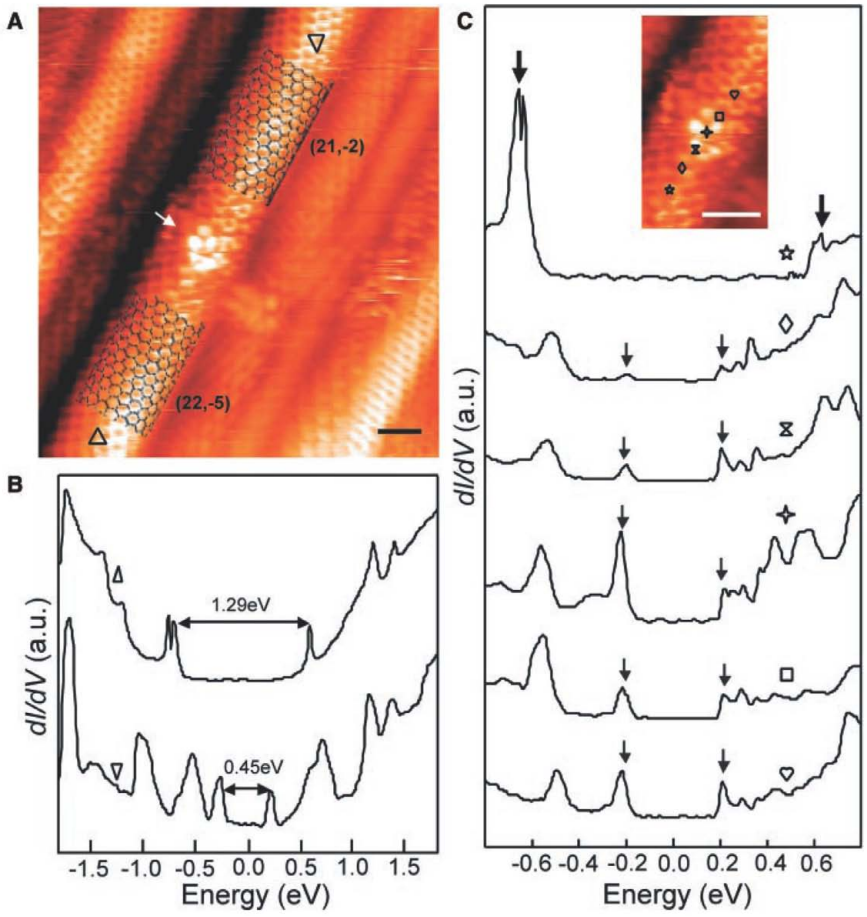


**Figure 1.** Structure and spectroscopy of a M-S IMJ. (**A**) Atomically resolved STM image of a SWNT containing an IMJ; the junction position is highlighted with a white arrow. Black honeycomb meshes corresponding to (21,–2) and (22,–5) indices are overlaid on the upper and lower portions, respectively, of the nanotube to highlight the distinct atomic structures of these different regions. The image was recorded in the constant-current mode with electrochemically etched tungsten tips at bias voltage $V_b = 650$ mV and $I = 150$ pA. Bar, 1 nm. (**B**) Tunneling conductance, *dI/dV*, recorded at the upper (∇) and lower (Δ) locations indicated in (A). The data were recorded directly as the in-phase component of the current *I* by a lock-in amplifier with a 7.37-kHz modulation signal of 2-mV peak-to-peak amplitude, and the curves presented in the figures were typically averaged over six sets of raw data. The energy difference between first VHS gap in the upper semiconducting segment, 0.45 eV, and lower metallic segment, 1.29 eV, are shown. (**C**) Spatially resolved *dI/dV* acquired across the M-S IMJ at the positions indicated by the six symbols on the high-resolution image (inset) of the junction interface. The small arrows highlight the positions of the first VHS of the semiconducting (21,–2) structure and emphasize their spatial decay across the junction; the large arrows highlight the first VHS of the metallic (22,–5) structure. Bar, 1 nm.

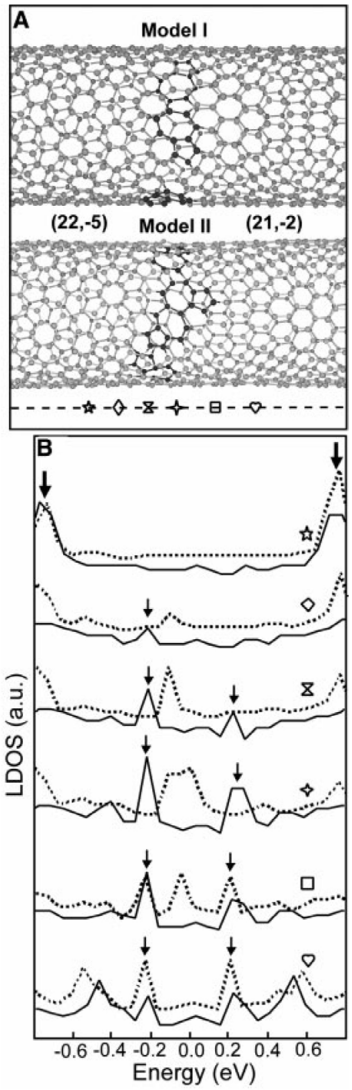


**Figure 2.** Atomic models and electronic properties of the M-S IMJ. (**A**) Two different models for a (22,– 5)/(21,–2) junction. Model I has three separated 5–7 pairs, and Model II has two isolated 5–7 pairs and one 5–7/7–5 pair. The filled black spheres highlight the atoms forming the 5–7 defects. The symbols in (A) are the same as in Figure 1A, and correspond to the locations where LDOS was calculated. (**B**) Calculated LDOS for Model I (solid line) and Model II (dashed line). More than 2000 carbon atoms were involved for calculation for every model. The small and large black arrows highlight the same features as in Figure 1C.

across the IMJ (Figure 3C) shows new features not observed in the M-S IMJ discussed above; that is, there are low-energy peaks at –0.55 and –0.27 eV not present in the spectroscopy data recorded away from the junction. These peaks appear to decay slowly from the IMJ into the bulk of the larger diameter segment but quickly into the smaller segment.

We determined the (n,m) indices of the larger and smaller segments of the IMJ structure using the iterative method above and find the best fits to be for values of (11,8) and (9,6), respectively, which are both metallic tubes. To check the consistency of this assignment, tight-binding calculations (25) were used to evaluate the LDOS for isolated (11,8) and (9,6) tubes. Comparison of the calculated and experimental LDOS (Figure 3B) shows excellent agreement and substantiates our assignment of the indices and the M-M character of the junction. The (11,8) and (9,6) SWNT segments can be joined seamlessly along a common axis using different configurations of 5–7 defects. A specific model (Figure 4A) we analyzed consists of two separated 5–7/7–5 pairs. It is also possible to connect the (11,8) and (9,6) segments using two or three 5–7 pairs, although our calculations suggest that these are less likely (26). The LDOS obtained from our π-only tight-binding calculation (Figure 4B) shows reasonable agreement with the experimental observation. Specifically, the low-energy peak at –0.55 eV matches that observed in experiment; however, we do not detect the other peak at –0.27 eV in our π-only calculations. We also evaluated and compared the decay of this peak in both directions from the IMJ and found that the calculated (1.6 $nm^{-1}$) and experimental (1.9 $nm^{-1}$) decay into the (9,6) segment agree better than calculated (2.6 $nm^{-1}$) and experimental (4.9 $nm^{-1}$) decay into the (11,8) segment.

We believe that the proposed atomic model represents a reasonable description of the IMJ but also realize that our calculations have limitations. In particular, the greater structural distortions required to join the (11,8) and (9,6) tubes probably require inclusion of at least 2s and 2p orbitals to describe properly the electronic structure. More detailed calculations should help to understand the origin of all of the localized states detected experimentally as well as the interesting asymmetry in the decay of these states from the IMJ interface.

The direct atomically resolved characterization of IMJs in as-grown SWNT materials by STM has important implications and opens exciting opportunities on several fronts. We have demonstrated unambiguously that IMJs are present in SWNT samples, and statistics show that topological defects occur with a relatively high frequency in these samples grown by laser ablation, in contrast to previous expectations. The common occurrence of these defects could have important implications for the interpretation of electrical transport and mechanical measurements. These studies provide experimentally derived atomic-level junction models that will enable an important dialog between experiments and further high-level calculations designed to reveal details of IMJ physics. We also believe that STM characterization of IMJs can provide critical information and a feedback

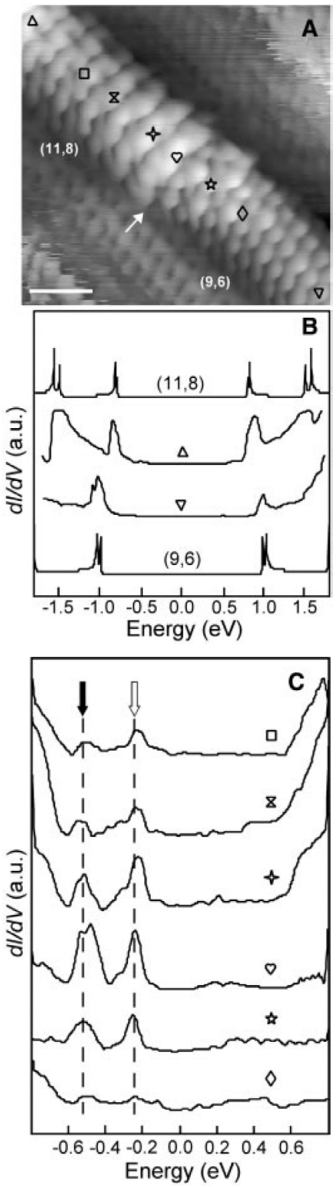


**Figure 3.** Structure and spectroscopy of a M-M IMJ. (**A**) Constant-current image of (11,8)/(9,6) junction recorded at $V_b$ = 500 mV and $I$ = 150 pA. The white arrow highlights the junction interface. Bar, 1 nm. Symbols are as in Figure 1, (A) and (C). The image of the upper SWNT segment is more complex than that found in typical data. Although detailed analysis is beyond the scope of this paper, recent calculations suggest that the observed structure in the image may be due to conduction electron scattering (22). (**B**) *dI/dV*, recorded at the upper (Δ) and lower (∇) locations indicated in (A). The corresponding calculated DOS for (11,8) and (9,6) SWNTs are shown above and below the experimental curves, respectively. (**C**) Spatially resolved *dI/dV* recorded across junction at the positions indicated in (A). New peaks at –0.55 and –0.27 eV in the junction region are highlighted by solid black and open arrows, respectively.

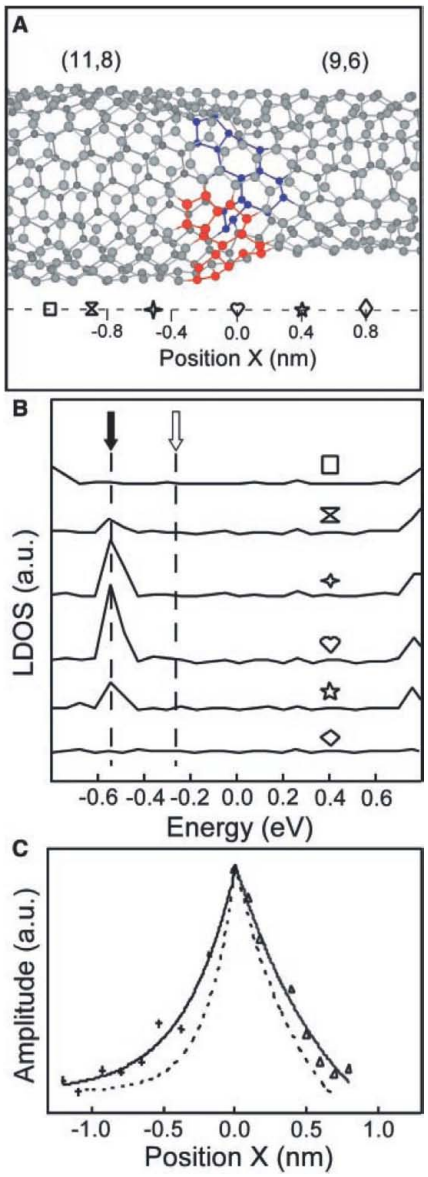


**Figure 4.** Atomic model and electronic properties of the M-M IMJ. (**A**) Model of the (11,8)/(9,6) junction containing two separated 5–7/7–5 pairs, which are highlighted with solid red and blue spheres. The view presented was obtained by rotating about the axis until the observed structure was similar to the experimental image (Figure 3A). (**B**) Calculated LDOS curves corresponding to the six positions indicated in (A). The solid black and open arrows correspond to the same positions highlighted in Figure 3C. (**C**) Spatial decay of the localized junction state at –0.55 eV. The solid and dashed lines correspond to fits to the experimental and calculated data, respectively. The origin, negative position [(11,8) side], and positive position [(9,6) side] are indicated in (A). The decay constants $k_d$ were obtained by fitting to $\exp[-k_d x]$.

mechanism for growth studies designed to establish rational pathways for controllably producing IMJs in the future.

### References & Notes


1. S. Saito, *Science* **278**, 77 (1997).
2. P. L. McEuen, *Nature* **393**, 15 (1998) .
3. C. Dekker, *Phys. Today* **52**, 22 (May 1999).
4. B. I. Dunlap, *Phys. Rev. B* **49**, 5643 (1994) .
5. Ph. Lambin, A. Fonseca, J. P. Vigneron, J. B. Nagy, A. A. Lucas, *Chem. Phys. Lett.* **245**, 85 (1995) .
6. L. Chico, V. H. Crespi, L. X. Benedict, S. G. Louie, M. L. Cohen, *Phys. Rev. Lett.* **76**, 971 (1996).
7. J.-C. Charlier, T. W. Ebbesen, Ph. Lambin, *Phys. Rev. B* **53**, 11108 (1996).
8. L. Chico, L. X. Benedict, S. G. Louie, M. L. Cohen, *Phys. Rev. B* **54**, 2600 (1996).
9. R. Saito, G. Dresselhaus, M. S. Dresselhaus, *Phys. Rev. B* **53**, 2044 (1996) .
10. J. Han, M. P. Anantram, R. L. Jaffe, J. Kong, H. Dai, *Phys. Rev. B* **57**, 14983 (1998) .
11. Z. Yao, H. W. Ch. Postma, L. Balents and C. Dekker, *Nature* **402**, 273 (1999) .
12. P. G. Collins, A. Zettl, H. Bando, A. Thess, R. E. Smalley, *Science* **278**, 100 (1997).
13. J. W. G. Wildoer, L. C. Venema, A. G. Rinzler, R. E. Smalley, C. Dekker, *Nature* **391**, 59 (1998).
14. T. W. Odom, J.-L. Huang, P. Kim, C. M. Lieber, *Nature* **391**, 62 (1998) .
15. T. W. Odom, J.-L. Huang, P. Kim, C. M. Lieber, *J. Phys. Chem. B* **104**, 2794 (2000) .
16. For example, a recent STM study suggests that the bend in a SWNT tube is an IMJ [ L. C. Venema, *et al*., *Phys. Rev. B* **62**, 5238 (2000) ]. However, the absence of atomic resolution makes it impossible to distinguish whether the observed "kink" connects two different tubes rather than corresponding to a simple bend. In addition, the VHS peaks above and below the bend are not consistent with the SWNT diameters. Hence, it is possible that the observed spectroscopic features are due to effects of bending (15).
17. T. W. Odom, J.-L. Huang, P. Kim, M. Ouyang, C. M. Lieber, *J. Mater. Res.* **13**, 2380 (1998).
18. M. Ouyang, J.-L. Huang, C. M. Lieber, unpublished data.
19. V. Meunier, P. Senet, Ph. Lambin, *Phys. Rev. B* **60**, 7792 (1999).
20. V. Meunier, Ph. Lambin, *Phys. Rev. Lett.* **81**, 5588 (1998).
21. D. Orlikowski, M. B. Nardelli, J. Bernholc, C. Ronald, *Phys. Rev. Lett.* **83**, 4132 (1999) .
22. A. Rubio, *Appl. Phys. A* **68**, 275 (1999) .
23. D. Orlikowski, M. B. Nardelli, J. Bernholc, C. Roland, *Phys. Rev. B* **61**, 14194 (2000) .
24. M. S. Dresselhaus, G. Dresselhaus, P. C. Eklund, *Science of Fullerenes and Carbon Nanotubes* (Academic Press, San Diego, 1996).
25. P. Kim, T. W. Odom, J.-L. Huang, C. M. Lieber, *Phys. Rev. Lett.* **82**, 1225 (1999).
26. Preliminary tight-binding calculations for these two models do not exhibit good agreement with experiment (18).


27. We thank M. S. Gudiksen, T. W. Odom, H. Park, and P. Kim for helpful discussion. Supported by the NSF.